JAAS

PAPER

View Article Online
View Journal | View Issue

Cite this: J. Anal. At. Spectrom., 2025, 40, 3306

Exploring age-induced lithium isotope fractionation in lithium-ion batteries using microwave-induced cold nitrogen plasma mass spectrometry

Dalia Morcillo, [ab] Alexander Winckelmann, [ab] Marcus Oelze, [a] Robert Leonhardt, [ac] Anita Schmidt,[a] Silke Richter, [a] Sebastian Recknagel,[a] Jochen Vogl, [a] Ulrich Panne [ab] and Carlos Abad *[a]

This study explores Microwave-Inductively Coupled Atmospheric-pressure Plasma Mass Spectrometry (MICAP-MS) as a cost-effective alternative to Multi-Collector Inductively Coupled Plasma Mass Spectrometry (MC-ICP-MS) for analyzing lithium isotopic composition in lithium-ion batteries (LIBs). We investigate the performance of MICAP-MS in measuring Li isotope ratios in new and aged commercial lithium cobalt oxide (LCO) batteries. Our results show that MICAP-MS, operating under cold plasma conditions at 800 W with an 8 mm torch position, achieves results metrologically compatible with MC-ICP-MS, with a precision ranging from 0.6‰ to 3.4‰ for δ^7Li values. MICAP-MS benefits from a dielectric resonator for uniform plasma, better ion velocity control, and higher energy efficiency. Optimal settings were identified with dwell times of 10 ms for ^{6}Li and 1 ms for ^{7}Li. The study of LIBs revealed that ^{6}Li migrates towards the anode over multiple charge–discharge cycles, causing ^{7}Li to accumulate in the cathode, a fractionation effect that becomes more pronounced with prolonged cycling. MICAP-MS provides a cost-effective, precise alternative to MC-ICP-MS, with lower operational costs and enhanced portability, advancing the study of isotopic fractionation and aging in lithium-ion batteries.

Received 6th September 2024
Accepted 4th August 2025

DOI: 10.1039/d4ja00324a

rsc.li/jaas

1. Introduction

Lithium-ion batteries (LIBs) have revolutionized portable electronics and electric vehicles since their commercialization in 1991 due to their high energy density, efficiency, and rechargeability. However, LIBs are subject to aging, which limits their lifespan. Understanding the mechanisms behind battery aging is crucial for improving their performance and longevity.[1]

An attribute associated with LIB aging is lithium isotope fractionation, a phenomenon where the ratio of lithium isotopes (^{6}Li and ^{7}Li) changes over time. This fractionation can result from structural changes in batteries and may be correlated to efficiency and capacity. It has been observed that the heavier isotope, ^{7}Li, tends to accumulate in the electrolyte, while the lighter ^{6}Li migrates towards the anode during charge–discharge cycles.[2–4] This isotopic distribution may serve as a window of the battery's performance and presents itself as a proxy of the aging process; however, this has not been well studied and established.

Traditionally, lithium isotope amount ratios (hereafter isotope ratios) have been measured using Thermal Ionization Mass Spectrometry (TIMS), which offers high accuracy but is limited by long analysis times and the potential for isotopic fractionation during measurement.[5] Multi-Collector Inductively Coupled Plasma Mass Spectrometry (MC-ICP-MS) has become the standard method for lithium isotope analysis due to its ability to simultaneously measure multiple isotopes with high precision.[6,7] However, MC-ICP-MS is not without drawbacks, including sensitivity to matrix effects and the requirement for high-purity argon gas, which significantly increases operational costs, as demonstrated by gas flow rate calculations by You *et al.*[8]

A microwave-induced nitrogen plasma ionization source offers a promising alternative for lithium isotope analysis used in nitrogen microwave inductively coupled atmospheric-pressure plasma mass spectrometry (MICAP-MS).[9,10] Unlike traditional ICP sources, MICAP uses nitrogen as the plasma gas, significantly reducing costs and eliminating the need for argon.[11,12] The MICAP system employs a dielectric resonator to generate a stable and homogeneous plasma, which improves ionization efficiency for many elements and minimizes issues such as secondary discharges common with traditional ICP sources.[13]

[a]Bundesanstalt für Materialforschung und -prüfung (BAM), Richard-Willstätter-Str. 11, D-12489 Berlin, Germany. E-mail: Carlos.Abad@bam.de
[b]Humboldt Universität zu Berlin, Department of Chemistry, Brook-Taylor-Str. 2, D-12489 Berlin, Germany
[c]Department of Energy and Automation Technology, Technische Universität Berlin, Einsteinufer 11, D-10587 Berlin, Germany

A key innovation in our approach is using a single quadrupole mass analyzer with MICAP-MS, instead of the more complex and expensive multi-collector systems typically used for high-precision isotope analysis. The single quadrupole setup, traditionally considered less precise for isotope ratio measurements due to the sequential measurement,[14,15] benefits significantly from the enhanced stability and efficiency of the MICAP ionization source. The stability of the MICAP plasma reduces the variability in ionization, leading to more consistent ion signals and improved measurement precision. A detailed explanation of the operation of the ion source can be found in previous research.[16]

This study investigates the application of MICAP-MS with a quadrupole single detector for analyzing lithium isotope fractionation in commercial lithium cobalt oxide (LCO) batteries. By comparing new and aged batteries, we aim to understand how lithium isotope ratios change over the lifespan of a battery. Using MICAP-MS, we strive to achieve acceptable precision in δ^7Li measurements, focusing on the isotopic changes occurring due to prolonged cycling and aging.

2. Experimental section

2.1. Materials and sample preparation

Four commercial pouch cell LIBs composed of lithium cobalt oxide (LCO) were investigated. The batteries had capacities ranging from 0.7 mAh to 1.75 mAh and operated within a 2.5 to 4.35 V voltage range. The maximum charging rate was estimated to be 2.1 A. Two of the batteries were aged to study the differences in the lithium isotope ratio between newly manufactured and end-of-life batteries. The aging was performed in a battery cycler MCT-HD system (Digatron Power Electronics, Germany) (Fig. 1A). For the charging cycle, a current of 1 A was used in constant current mode until 4.35 V was reached, charging at a constant voltage of down to 50 mA. This charging cycle was followed by the discharge cycle with a current of 1 A until 2.5 V was reached. The electrochemical impedance of the resistivity of the battery to current disturbance was performed with an Interface 5000E potentiostat (Gamry Instruments, USA). Fig. 1B shows the electrochemical impedance spectra of the battery after 0 to 210 cycles. The impedance spectra increase slightly from 0 to150 cycles corresponding to the formation of the passivation layers and indicating a normal degradation. However, after 150 cycles, a significant rise in impedance and ohmic resistance ($Z'' = 0$) suggests a loss of usable lithium ions.

Once discharged to the cut-off voltage, the batteries were opened under normal temperature and pressure (NTP) conditions. The anodes were separated from the cathodes and the separator. In total, two anodes (NEW-A1, NEW-A2) and two cathodes (NEW-C1, NEW-C2) were obtained from the new batteries, and two anodes (AGED-A1, AGED-A2) and two cathodes (AGED-C1, AGED-C2) from the aged batteries.

Approximately 0.5 g of cathode and anode material of each battery were separated from the aluminum and copper current collectors by mechanical scraping using a metal spatula. To ensure the removal of graphite from the sample, the powdery cathode and anode materials were placed in platinum crucibles and calcinated in a muffle furnace at 1100 °C for 1 h. After that, the samples were digested at 150 °C for 2 h with 16 mL aqua regia. For this, HNO_3 (Merck, Germany) and HCl (Merck, Germany) were previously purified by sub-boiling distillation in PFA containers. High-purity deionized water with a resistivity of 18 MΩ cm obtained from a Milli-Q system (Merck Millipore, Germany) was used throughout the experiments. After digestion of the active material, the solution was diluted to 100 mL with deionized water and used for ICP-OES control analysis (Tables S3 and S4).

To avoid spectral interferences, the sample matrix was removed. Consequently, lithium was quantitatively separated from the transition metals by ion-exchange chromatography (IC) as previously described.[17] The IC column, made of polypropylene with a length of 20.5 cm and a diameter of 8 mm, was filled with 3 mL of AG-50W-X8 resin (analytical grade, BIO-RAD). The preparation of the column, based on the Van Hoecke *et al.* procedure,[18] is detailed in Table S1. A standard solution was prepared according to the cathode composition to check the efficiency of the columns. The standard cathode solution, containing 2.5 mg L^{-1} of Li, 7 mg L^{-1} of Al, and 20 mg L^{-1} of Co, was loaded onto the column with a volume of 2 mL.

To determine the range of the mobile phase for lithium, 15 fractions with 2 mL of eluate each and an extra fraction with the

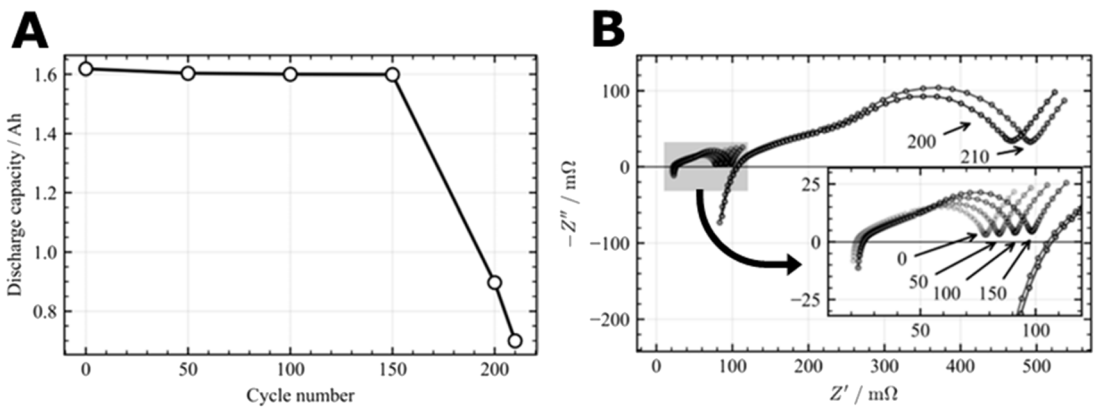

Fig. 1 (A) Measured battery capacity *vs.* number of charge/discharge cycles. (B) Impedance response of the aged battery over the aging cycles, where the *x*-axis is the real component, and the *y*-axis is the imaginary component.

remaining eluate were collected and filled up to 10 mL with 2% nitric acid (HNO_3). Fig. T1, in SI, shows how the eluted lithium appears between fractions 4 and 11 separated from Co and Al. The IC process was subsequently applied to the battery samples (Table S2). The sample preparation process is represented in Fig. 2. Each isotope-ratio replicate consumed only ≈2 ng Li (0.20 mL of a 10 μg per L eluate), *i.e.*, <0.00001% of the ≈25 mg Li dissolved from a 0.50 g cathode sample and <0.0001% of the ≈2 mg Li dissolved from a 0.50 g anode sample. For this type of LCO battery material, calcination at 1100 °C does not introduce measurable lithium isotope fractionation, as lithium remains in stable, low-volatility oxide forms (*e.g.*, $LiCoO_2$) with vapor pressure well below levels that would induce volatilization or Rayleigh distillation.[19]

2.2. ICP-optical emission spectrometry measurements

Before measurements using MC-ICP-MS and MICAP-MS, the Li concentrations of the samples were determined by ICP-optical emission spectrometry (OES) using an Agilent 5110 ICP-OES equipped with an automatic sampling system SPS 4 (Agilent Technologies Australia Pty Ltd, Australia). Calibration was performed from 50 to 500 μg per L Li at a wavelength of 670.783 nm in axial mode using certified single-element stock solutions, a Li ICP Standard (Certipur®), or an ICP multi-element standard solution (ICP multi-element standard solution IV Certipur®), depending on the sample matrix. The instrument parameters are provided in Table S3.

2.3. Instrumental conditions and validation of MICAP-MS

A PlasmaQuant MS Elite quadrupole mass spectrometer (Analytik Jena GmbH, Germany) modified with an inductive microwave plasma source was used for all experiments. Nitrogen (N_2 purity ≥99.999%, Linde AG, Germany) was used as a nebulizer, auxiliary, and plasma gas. A peristaltic pump was used to transport the liquid samples to a concentric nebulizer (MicroMist, USA) combined with a cooled double-pass spray chamber at 3 °C. A 2.45 GHz microwave is generated from a microwave oven magnetron and coupled to a dielectric resonator ring to sustain the plasma.[16]

The optimum time to achieve a stable $^7Li/^6Li$ ratio signal was 120 s. The parameters of the ion optics (lens and mirror voltages) were adjusted to obtain high sensitivity based on recent research.[11] Finally, the effect of the skimmer bias was also optimized, obtaining a stronger lithium signal at 3 V skimmer bias.

Instrumental parameters like plasma power, dwell time, sample time, data acquisition, and skimmer bias were tested to achieve a more stable lithium signal. Table 1 presents the detailed parameters for lithium isotope analysis.

Two samples were selected for quality control using MC-ICP-MS: lithium carbonate (Fluka, Germany) and lithium fluoride (Merk, Germany), and two certified reference materials (CRMs): NIST SRM® 8545 (NIST, USA), usually referred to as LSVEC, which defines the lithium delta scale and, by definition, has a δ^7Li value of 0‰, and a second certified lithium carbonate IRMM-016 (European Commission JRC, Belgium).

The lithium isotopic compositions (δ^7Li), reported in per mille (‰) deviations from LSVEC, were measured by MC-ICP-MS, as defined in eqn (1). The solutions were measured using standard-sample bracketing with LSVEC, and a blank measurement was taken before each standard and each sample. The solutions were prepared as previously described,[17] and detailed sample information is provided in Table S5. To match a ^{6}Li signal of 95 000 counts per second (c per s) and a ^{7}Li signal of 1 200 000 c per s a lithium concentration solution of 10 μg L^{-1} was used.

$$\delta^7\mathrm{Li} = \delta^{7/6}\mathrm{Li}_{\mathrm{LSVEC}} = \left(\frac{\overline{R}\left(\frac{^7\mathrm{Li}}{^6\mathrm{Li}}\right)_{\mathrm{sample}}}{\overline{R}\left(\frac{^7\mathrm{Li}}{^6\mathrm{Li}}\right)_{\mathrm{LSVEC}}} \right) - 1 \quad (1)$$

Table 1 Instrumental parameters for Li isotope analysis using MICAP-MS

MICAP-MS	
Plasma power	800 W
Nebulizer gas flow	1.35 L per min N_2
Auxiliary gas flow	1.8 L per min N_2
Plasma gas flow	11 L per min N_2
Sampling depth	5 mm/8 mm
Sampling cone	Pt 1.1 mm
Skimmer cone	Ni 0.5 mm
Dwell time	0.1 s
Sample time	345 s
Dwell time ^{7}Li/^{6}Li	1 : 10
Point/peak	1

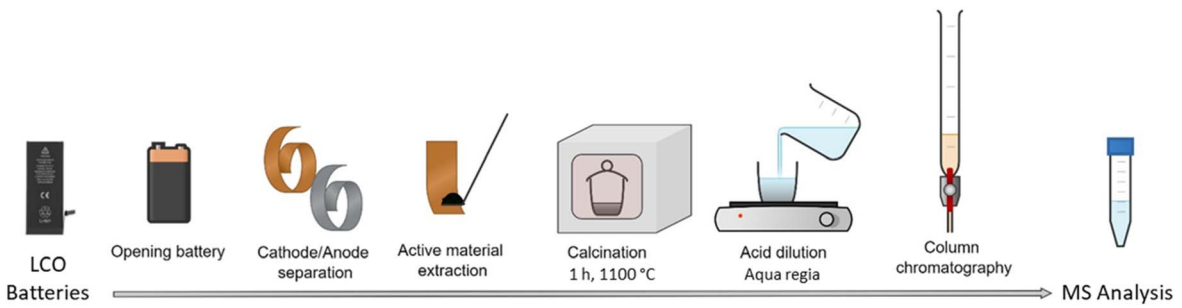

Fig. 2 Battery sample preparation for Mass Spectrometry (MS) analysis with matrix extraction.

2.4. MC-ICP-MS measurements

Measurements of δ^7Li values for the set of validation samples were carried out using a Neptune Plus MC-ICP-MS instrument (Thermo Fisher Scientific, Bremen, Germany) in standard configuration. The corresponding instrument parameters can be found in our previous work,[16] except that the battery samples in this study were measured using Al cones instead of Ni cones. By using a lithium mass fraction of about 0.5 mg kg^{-1}, an average signal intensity of 12 V was obtained for lithium, and the typical repeatability for lithium isotope ratio measurements was about 0.1‰. The samples were diluted with nitric acid ($w(HNO_3) = 20$ g kg^{-1}). Each sample was measured at least two to three times with 40 cycles. The representative drift between two consecutive bracketing standards in the ^{7}Li/^{6}Li ratio was 0.1–0.2‰.

3. Results and discussion

To achieve the detection of a robust signal for lithium isotope with precision comparable to ICP-MS (≤0.6‰ by single collector triple quadrupole ICP-MS[20]) and to study the sensitivity and mass bias for lithium isotope analysis, the conditions for MICAP-MS have been tested. The selection of the parameters focused on three criteria: achieving a higher Li signal for both isotopes, maintaining plasma stability, and ensuring the isotope ratio is closer to the natural value of the ^{7}Li/^{6}Li ratio, which would suggest lower mass bias from the equipment.

3.1. Selection of instrumental conditions

The quadrupole-based ICP-MS instruments are limited to dwell times in the millisecond range and have a data acquisition overhead that negatively affects data quality.[21] In contrast to the MC-ICP-MS, whose multicollector allows a simultaneous ion measurement, MICAP-MS performs a sequential detection of the ions generated in the plasma. In the worst-case scenario, sequential detection could measure the first isotope at the highest intensity and the second isotope at the lowest intensity in an assumed sinus-like fluctuation of the intensity. This difference can lead to significant variations in ion intensity being directly transferred to the isotope ratio, negatively affecting the accuracy of the measurement. To minimize this drawback of sequential detection, an optimal measurement time adjustment is crucial to achieving a stable signal.[22]

The bias between measured and reference values was investigated using LSVEC with a lithium concentration of 10 µg L^{-1} to set dwell time, data acquisition points, and sample time. The results are shown in Fig. 3 and more detailed in Table S6.

Firstly, dwell times for both Li isotopes ranging from 100, 1000, 10 000 to 100 000 µs were tested for a total data acquisition time (sweep time) of 250 s (Fig. 3A). The instrument selected 70 scans for 100 µs dwell time, 50 scans for 1000 µs, 18 scans for 10 000 µs, and 10 scans for 100 000 µs (Table S6). The number of scans decreases as dwell time increases to maintain a constant sweep time. This is because, for quadrupole-based MS, the sweep time is equal to the sum of dwell and settling times (the time that a mass spectrometer (MS) pauses after finishing a cycle until it begins the next cycle).[23] The most precise result was obtained with a dwell time of 10 000 µs for an instrumental isotope fractionation of −0.74. While shorter dwell times are in theory ideal for minimizing the effects of the sequential detector, the signal might not have enough time to

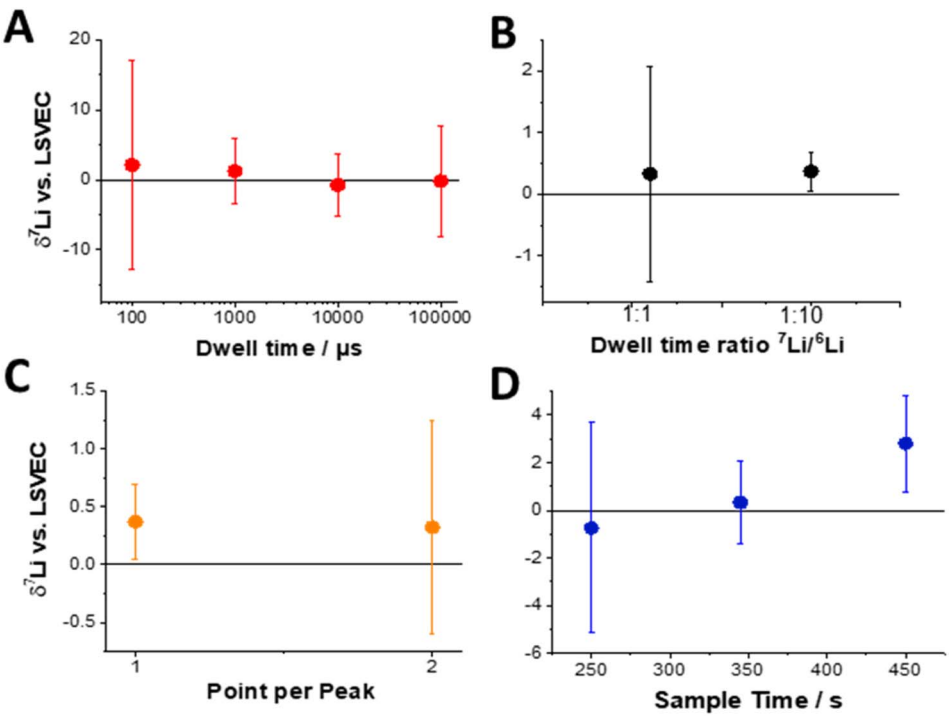

Fig. 3 Bias between measured and reference values for setting conditions of dwell time for both isotopes in (A), dwell time for the ^{7}Li/^{6}Li ratio (B), data acquisition points (C) and sweep time (D).

accumulate sufficiently at these shorter dwell times, leading to a lower signal-to-noise ratio.

To determine the optimal sweep time, sweep times of 250 s, 345 s, and 450 s were tested with a fixed dwell time of 10 000 μs, resulting in scans of 18, 70, and 100, respectively (Fig. 3D). The lowest standard deviation was observed with a sweep time of 345 s. For lithium isotope analysis, sweep time is most efficient with an increased number of scans (over 70 scans/replicate). A sweep time of 250 s may be insufficient to detect each isotope. Increasing the sweep time to 345 s while maintaining the same dwell time significantly improves the accuracy. However, it still does not provide enough time to accumulate the less abundant isotope, ^{6}Li. The ratio ^{7}Li/^{6}Li shows an increasing tendency with increasing sweep time (Fig. 3D). This effect may be explained by the total measurement time. A slight increase (<0.4‰) in the ^{7}Li/^{6}Li ratio with longer sweep time (Fig. 3D) is attributed to residual count-rate-dependent artifacts,[14,24] primarily incomplete dead-time correction and space-charge defocusing, which subtly favor the more abundant ^{7}Li during extended integrations. At the selected 345 s sweep time, the projected bias is <0.05‰, well below the method's ± 0.6‰ external precision and thus negligible.

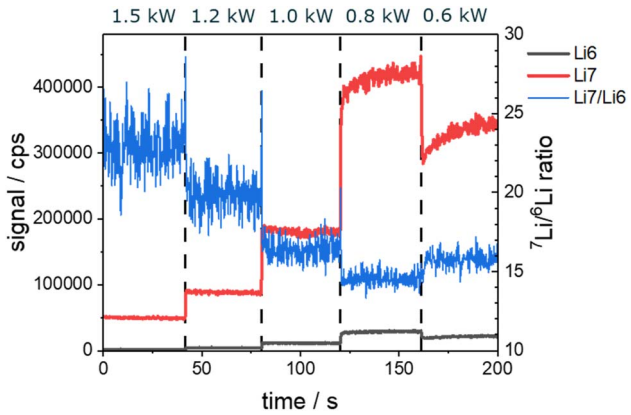

Fig. 4 Comparison of the lithium signal for a plasma energy setting range from 1500 W to 600 W.

The dwell time on the isotopic ratio ^{7}Li/^{6}Li was then selected, keeping the previous dwell time of 10 000 μs constant for ^{6}Li, while the dwell time of ^{7}Li was modified for 1 : 1 and 1 : 10 ^{7}Li/^{6}Li ratios. The 1 : 10 ratio resulted in the most reliable dwell time (Fig. 3B). These parameters allow a measurement time per isotope much lower than the period of the oscillation/noise T, avoiding a negative influence on the isotope ratio precision.

Finally, the number of points per peak of data acquisition was tested. The most precise result (Fig. 3C) was obtained with the acquisition of 1 point per peak, for which 94 scan replications were used. Increasing the number of points per peak while maintaining a fixed sweep time reduces the total number of scans, limiting statistical averaging of signal fluctuations and thereby increasing bias and uncertainty, as observed in our tests (Table S6). This trade-off is well-documented in quadrupole ICP-MS for isotope ratio measurements.[25,26]

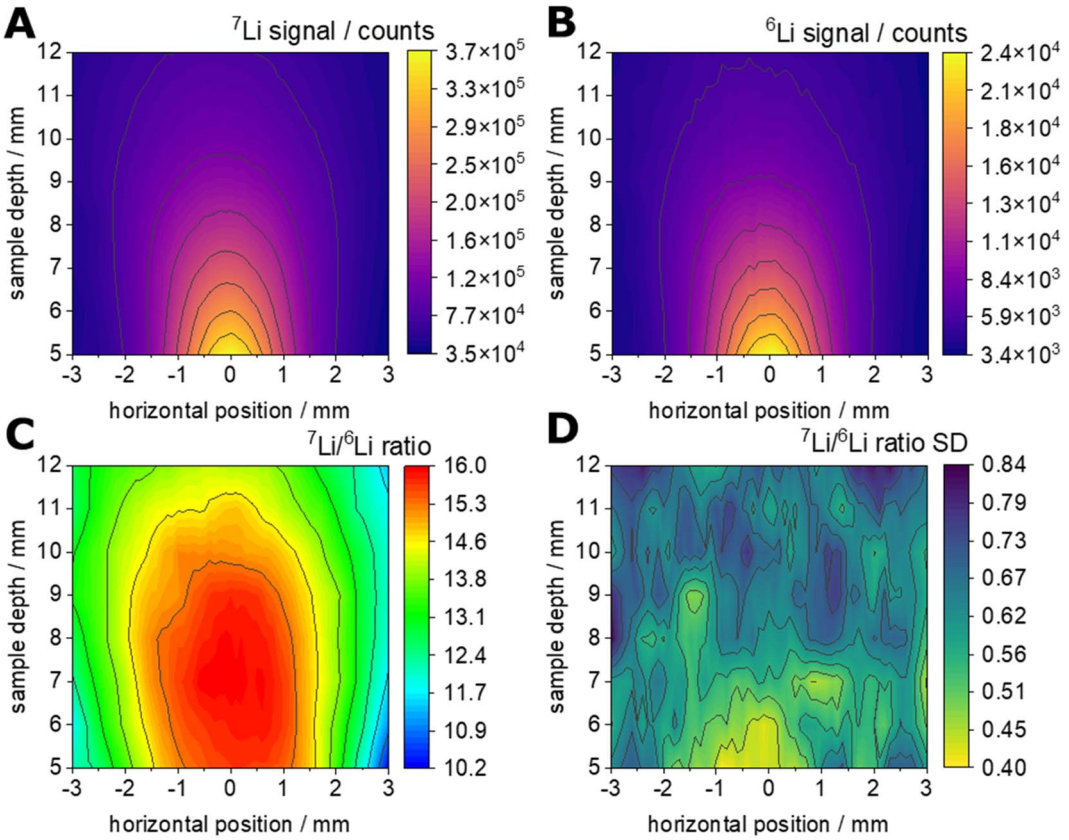

Fig. 5 Analysis of plasma signal intensity and isotopic ratio for ^{7}Li and ^{6}Li under hot plasma conditions (1500 W). (A and B) Represent the signal intensity for ^{7}Li and ^{6}Li, respectively. (C) Illustrates the ^{7}Li/^{6}Li ratio, and (D) shows the standard deviation of 10 measurements per location.

In conclusion, the results of the detailed parametric study (indicated in Table S6 with a grey band): dwell time of 10 000 μs for ^{6}Li and 1000 μs for ^{7}Li, sweep time of 345 s, and 1 point per peak in the data acquisition allow measurements of lithium isotopes with intensities close to each other and short measurement times. This means that the disadvantages of sequential quadrupole detection are limited under these conditions. This fact and the stability of the nitrogen source plasma of the MICAP-MS provide a stable signal, improving the precision of the isotope ratio.

3.2. Effect of plasma power

Atmospheric plasma torches in MICAP-MS generate plasma at very high temperatures under atmospheric pressure.[16] However, higher plasma temperatures do not always result in more efficient ionization and extraction of analytes. For ICP-MS, cold plasma conditions lead to a higher signal for light and easily ionizable elements such as lithium, sodium, and potassium.[27] In this section, different plasma power settings from 1500 W to 600 W were investigated.

As shown in Fig. 4, cold plasma conditions at 800 W forward power were considered optimal. The signal intensity for both isotopes is higher than using other power settings, and their isotope ratio is more stable and closer to the natural ^{7}Li/^{6}Li ratio value of 12.7.

The enhancement of lithium intensity observed with cold plasma (800 W) can be attributed to the optimal plasma temperature, which promotes lithium ionization.[20] This is particularly significant considering lithium's relatively low ionization energy, which stands at 5.4 eV.

A higher plasma energy level would facilitate the ionization of doubly charged ions derived from isobaric interferences like $^{12}C^{2+}$ and $^{14}N^{2+}$, generating more interferences in the lithium signal and lower ionization efficiency (see Fig. T2 for mass scans of a blank solution measured at different plasma power levels). Therefore, by using low-energy plasma conditions, interference from these doubly charged ions can be minimized. This allows a more accurate and precise measurement of lithium isotope ratios.

Additionally, cold plasma energy creates a more focused ion stream, resulting in less isotopic fractionation of ^{7}Li and ^{6}Li. Together with the intrinsically stable nitrogen plasma source, this setup provides sub-percent signal RSD, supporting the per-mille range external precision achieved with our bracketing protocol. The coil-less dielectric-resonator design, as detailed by Jevtic *et al.*,[13] has demonstrated sub-percent stability in independent studies,[9,28] reinforcing the reproducibility reported here.

3.3. Effect of torch position

Nonuniformities in the plasma can impact the quality of sample ionization. Areas of the plasma with higher electron density absorb more power than areas with lower electron density,

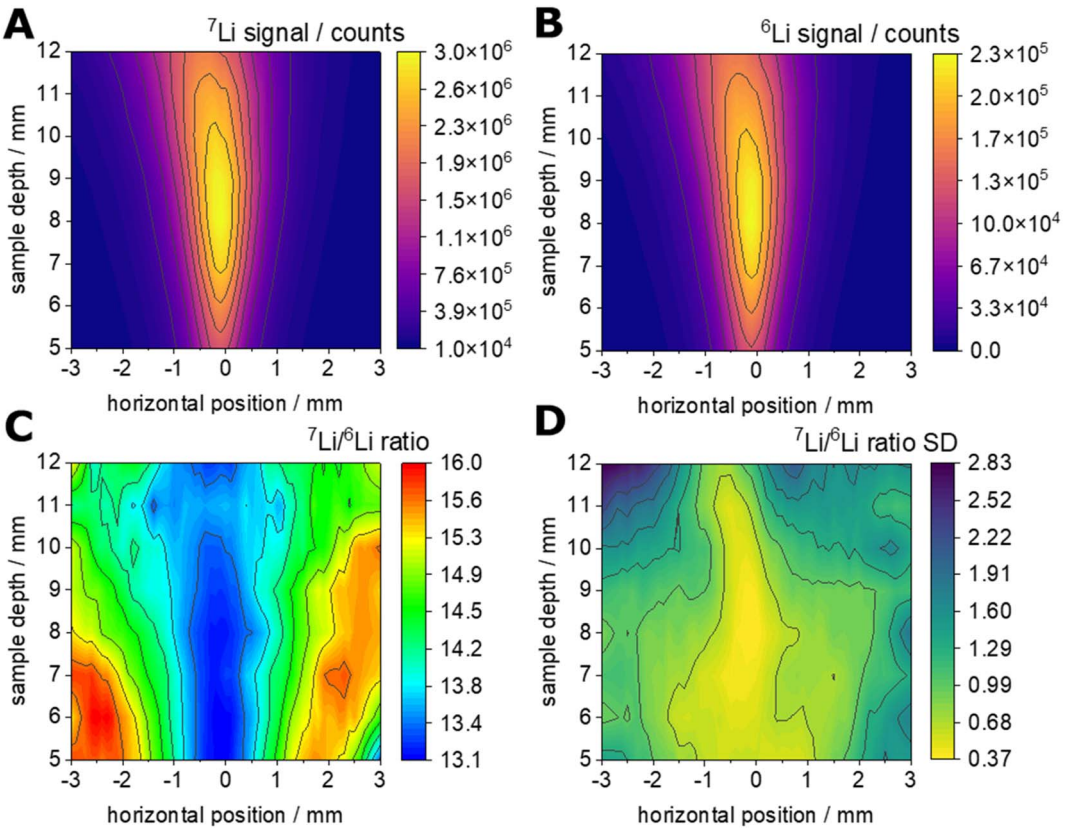

Fig. 6 Analysis of plasma signal intensity and isotopic ratio for ^{7}Li and ^{6}Li under cold plasma conditions (800 W). (A and B) Represent the signal intensity for ^{7}Li and ^{6}Li respectively. (C) Illustrates the ^{7}Li/^{6}Li ratio, and (D) shows the standard deviation of the measurements.

resulting in different ionization levels in these regions and these variations can cause plasma instability. The effect of the torch position was studied to find the most stable plasma region for lithium isotopes. The sample depth in the plasma was modified from 5 to 12 mm, and the horizontal torch position varied from −3 to 3 mm. For this purpose, 10 replicates were scanned along the horizontal position for each sample depth. The contour plots (Fig. 5 and 6) show the spatial distribution of plasma properties at two different plasma energies of 1500 W (hot plasma) and 800 W (cold plasma), respectively.

Fig. 5A and B suggest that the area of the highest signal of ^{7}Li and ^{6}Li can be detected at the smallest sample depth of 5 mm. The Li signal steeply decreases in all directions. This may indicate a strong electrostatic repulsion of the light Li^+ ions from the more abundant ion species present in the hot plasma, namely N^+, O^+, N_2^+, NO^+, *etc.*

In Fig. 5C, a high ^{7}Li/^{6}Li ratio is observed at the middle position near the lowest depth of the sample, where the value significantly deviates from the natural value of 12.17. The ratio decreases towards the outer side and with increasing sample depth, indicating both a stronger electrostatic repulsion for the lighter ^{6}Li, leading to isotopic fractionation within the plasma, and strong interference from doubly charged nitrogen.

The small area with a low standard deviation of the ratio, as shown in Fig. 5D, overlaps with the area of highest intensity (Fig. 5C) at this torch position. However, in this zone, a higher isotopic fractionation is found.

In conclusion, for the 1500 W plasma power conditions, there are regions within the plasma where the ionization of ^{7}Li and ^{6}Li differs significantly, making it difficult to obtain consistent and accurate isotopic measurements.

Fig. 6A and B show a large area at the torch position with a higher Li signal for both isotopes in cold plasma power conditions. Within the position range, these figures indicate that the most stable plasma region is at an 8 mm sample depth and a horizontal torch position of 0 mm for both lithium isotopes. The cold plasma condition produces a more focused ion cloud with less electrostatic repulsion. This stability may be produced by a more efficient energy transfer from the plasma source at this depth, increasing the ionization of both ^{7}Li and ^{6}Li.

Fig. 6C shows the closest to the natural ^{7}Li/^{6}Li ratio in a large central area at a sample depth of 5 mm to 9 mm. This may indicate the absence of isotopic fractionation in this zone and a very low background of doubly charged nitrogen and carbon. This only affects the ratio at the horizontal ends, where the Li signal is low.

Mapping along the different torch positions, Fig. 6D reveals a large central area with the lowest standard deviation for the isotope ratio, matching the area of the highest Li signal and less isotope fractionation. This uniformity leads to greater plasma stability, crucial for achieving precise isotopic analysis and confirming that cold plasma power conditions at 8 mm sample depth provide a uniform and homogeneous plasma environment.

3.4. Quality control

Table 2 compares the results from the method validation using MC-ICP-MS and MICAP. The MICAP achieved a precision between 1‰ and 2.5‰ for δ^{7}Li. The metrological compatibility of MICAP data is calculated concerning the δ^{7}Li values from MC-ICP-MS, by applying the E_n value.[29] Values are considered metrologically compatible when $E_n < 1$.

To study the repeatability of this method, the IRMM-016 was measured against LSVEC by applying standard-sample bracketing over 6 days. The mean IRMM-016 δ^{7}Li value over 6 days was 0.65 with a precision of 1.99‰. The repeatability results are shown in Fig. 7.

3.5. Battery analysis

After the selection of optimal conditions and method validation, the battery samples were measured using cold plasma MICAP-MS. Table 3 compares the MICAP and MC-ICP-MS

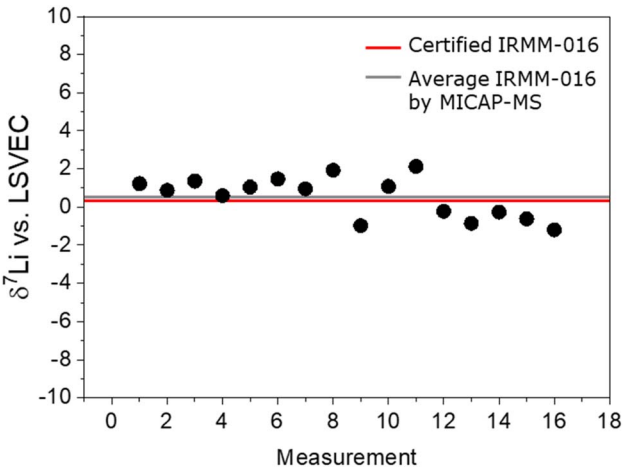

Fig. 7 δ^{7}Li values of reference material IRMM-016 during 6 days of measurements.

Table 2 δ^{7}Li of reference materials LSVEC, IRMM-016 and quality control samples LiF and Li_2CO_3[a]

	MICAP				MC-ICP-MS			
Name	δ^{7}Li *vs.* LSVEC/‰	2SD	*U*	*n*	δ^{7}Li *vs.* LSVEC/‰	2SD	*U*	E_n
LSVEC	0.10	1.40	2.29	15	0.00	0.12	0.47	0.07
Li_2CO_3	15.01	1.07	2.30	6	15.34	0.36	0.55	0.29
LiF	293.53	2.53	2.59	4	294.82	0.54	0.89	0.50
IRMM-016	0.65	1.99	2.32	15	0.07	0.70	0.57	0.28

[a] Uncertainties are reported as the standard deviation of the mean, with a coverage factor of $k = 2$, corresponding to a confidence level of 95%.

Table 3 δ^7Li of anodes and cathodes from 2 new and 2 aged LCO commercial batteries, and LSVEC using MICAP compared to MC-ICP-MS[a]

		MC-ICP-MS			MICAP			
	Name	δ^7Li *vs.* LSVEC/‰	2SD	*U*	δ^7Li *vs.* LSVEC/‰	2SD	*U*	E_n
New battery 1	NEW-A1	23.49	0.02	0.57	23.28	3.00	2.71	0.07
	NEW-C1	4.32	0.07	0.57	5.40	3.38	3.29	0.32
New battery 2	NEW-A2	16.74	0.21	0.64	17.50	0.92	2.32	0.81
	NEW-C2	4.84	0.02	0.56	4.6	1.67	2.46	0.15
Aged battery 1	AGED-A1	24.80	0.03	0.57	25.49	1.53	2.43	0.45
	AGED-C1	7.15	0.05	0.56	7.32	0.69	2.30	0.26
Aged battery 2	AGED-A2	22.35	0.02	0.57	23.07	1.27	2.38	0.56
	AGED-C2	6.80	0.28	0.69	7.61	1.68	2.46	0.47

[a] Uncertainties are reported as the standard deviation of the mean ($n = 4$), with a coverage factor of $k = 2$, corresponding to a confidence level of 95%.

results and their associated uncertainties. Values are considered metrologically compatible when $E_n < 1$. The results show metrological compatibility for all battery samples. The measurements of the samples were reproducible over 2 days according to the validation standard.[30]

Fig. 8 shows the δ^7Li values between newly manufactured and aged anodes. The experimental data supports the tendency of ^{7}Li accumulation in the aged cathodes and suggests a lack of disparity in isotopic composition between anodes and cathodes. While the box plots for the battery anodes (Fig. 8A) show a slight enrichment of ^{7}Li in the anode, where the solid electrolyte interface (SEI) could play the role of an ion exchange resin for Li^+ ions,[31] the box plots for cathodes of the aged batteries show a higher enrichment of ^{7}Li which starts to become significant (Fig. 8B). To obtain statistically relevant data, however, a larger number of new and aged batteries needs to be analyzed.

Due to their mass difference, lithium isotopes ^{6}Li and ^{7}Li can exhibit different behaviors during electrochemical processes.[32] This is known as the isotope effect, where lighter isotopes tend to move and react slightly faster than heavier ones due to their lower mass and higher mobility.[33]

LIBs are based on intercalation systems on the $LiCoO_2$ structure of the cathode and the graphite structure of the anode. During the lithium-ion battery's charging and discharging cycles, lithium ions move between the anode and the cathode through the electrolyte. Over time, due to the isotope effect, ^{6}Li, being lighter, will tend to diffuse slightly faster than ^{7}Li. This differential movement can gradually accumulate the heavier isotope ^{7}Li in different areas of the battery. As the battery ages and undergoes many charge/discharge cycles, the continuous and slightly preferential intercalation of ^{6}Li at the anode causes a relatively larger amount of ^{7}Li to end up at the cathode. This process is slow and cumulative, so it is only noticeable in older batteries. Over many cycles, these small differences add up, leading to the observed accumulation of ^{7}Li in the cathode.

Several investigations have demonstrated evidence of lithium accumulation in different battery locations: at the anode/current collector and cathode/electrolyte interfaces of all-solid-state lithium,[34] and at the anode/electrolyte interface during the formation of the solid electrolyte interface (SEI).[35] Additionally, deviations in stack geometry and the electrical connection of electrodes have been shown to affect the homogeneity of lithium distribution within the active materials of each electrode.[36] These cases of non-homogeneous lithium distribution could be related to the deposition of one of the isotopes in specific parts of the battery.

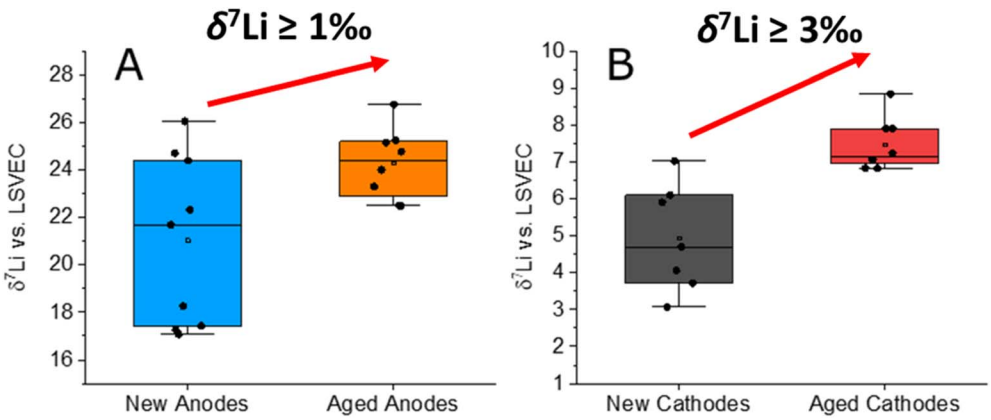

Fig. 8 δ^7Li values for new and aged anodes (A) and new and aged cathodes (B).

In addition, investigations on lithium isotopies in batteries demonstrated the preference for ^{7}Li to dissolve in the electrolyte.[3] However, the possible causes of isotopic fractionation in batteries have not yet been defined.

An accumulation of the heavier isotope ^{7}Li at the cathode could be due to a hindrance caused by intercalation in the cathode's layered structure. This Li intercalation hindrance in the LCO structure could be due to significant changes in the crystalline surface and electronic structures of $LiCoO_2$ cathodes after long-term battery storage[27] or to an active formation of the cathode-electrolyte interphase (CEI).[37]

4. Conclusions

The proposed technique provided results comparable with MC-ICP-MS for lithium isotope analysis with precision from 0.6‰ to 3.4‰. In MICAP-MS, similar to ICP-MS, the instrumental isotope fractionation depends on plasma conditions. However, the fractionation in MICAP-MS is smaller and more stable compared to ICP-MS. While the repeatability of δ^{7}Li measurements with MC-ICP-MS is 4 to 10 times better, and the measurement uncertainty is 3 to 5 times lower, MICAP-MS is still highly suitable for screening lithium δ-values due to its cost-effectiveness, sustainability, and operational simplicity compared to MC-ICP-MS.

Despite employing different ionization sources and mass analyzers, both MC-ICP-MS and MICAP-MS offer high precision for lithium isotope analysis in commercial batteries. However, the traditional coil used in the plasma generator of MC-ICP-MS has some coil-related limitations, such as an expensive and unportable cooling system, corrosion of the coil surface, and electrical potential differences between the coil turns. MICAP, however, employs a dielectric resonator ring coupled to a 2.45 GHz microwave field for a plasma generator.[16] A dielectric resonator ensures a more uniform plasma, better ion velocity control, and higher energy efficiency.

Operating the MICAP-MS under cold plasma conditions at 800 W and selecting a sampling depth torch position of 8 mm offer significant advantages in ionization efficiency, signal intensity, analytical performance, and plasma stability compared to hot plasma conditions. These benefits are essential for achieving accurate and reliable lithium isotopic analysis. The precision achieved with MICAP-MS is sufficient for monitoring lithium isotope fractionation in lithium-ion batteries during aging and cycling processes. Additionally, this level of precision is well-suited for broader applications, such as environmental studies and industrial monitoring, where high-throughput and cost-effective isotope analysis are required. The improved signal stability and intensity observed under optimized plasma conditions reflect the efficient ionization capability of MICAP-MS. Quantitative metrics, such as the useful ion yield, could further characterize its performance and will be an important focus for future studies.

For the selected setting conditions of the instrument, the dwell times of 10 000 μs for ^{6}Li and 1000 μs for ^{7}Li strike a balance between accumulating enough signal for a high signal-to-noise ratio and minimizing the short-term plasma fluctuations. The 1 : 10 ratio for the ^{7}Li/^{6}Li dwell time allows the mass detector to balance the lower abundance of ^{6}Li (7.493%) *vs.* ^{7}Li (92.507%) by accumulating the ^{6}Li isotope for a longer time. This balance results in the most precise δ^{7}Li measurements, as evidenced by the highest precision and reproducibility.

Analyzing new and aged batteries for their δ^{7}Li values reveals lithium isotope fractionation due to prolonged cycling, with a fractionation range of +8.0‰ for the anode and +3.0‰ for the cathode. This effect arises from the preferential migration of the lighter lithium isotope ^{6}Li towards the anode, causing the heavier isotope ^{7}Li to accumulate in the cathode as the battery ages. The fractionation becomes increasingly apparent with repeated charge–discharge cycles. Previous research has documented lithium isotopic fractionation at the cathode–electrolyte interface during lithium release, associated with battery charging reactions.[2,3] However, these earlier studies focused on half-cells rather than full batteries. In contrast, our work examines real batteries, capturing the interaction between the anode and cathode, providing a more comprehensive understanding of lithium isotope behavior during cycling.

The potential accumulation of ^{7}Li at the cathode of aged batteries warrants further investigation to understand the underlying causes of this phenomenon. Future studies could explore *in situ* and spatial resolved analysis under inert atmospheric conditions to avoid lithium oxidation, along with a systematic investigation of different aging states in LIBs to obtain further information on the exact onset of isotopic fractionation.

Applying MICAP-MS for lithium isotope analysis in LIBs provides a cost-effective and precise method for studying age-induced isotopic fractionation. This technique holds significant potential for improving our understanding of battery aging and guiding the development of more durable and efficient LIBs.

Author contributions

Dalia Morcillo: writing – review & editing, writing – original draft, validation, methodology, investigation, formal analysis, software, data curation. Alexander Winckelmann: writing – review & editing, visualization, formal analysis. Marcus Oelze: writing – review & editing, formal analysis, validation. Robert Leonhardt: resources, formal analysis. Anita Schmidt: writing – review & editing, resources, investigation. Silke Richter: funding acquisition, conceptualization. Sebastian Recknagel: writing – review & editing, supervision, resources, funding acquisition. Jochen Vogl: writing – review & editing, validation, methodology, formal analysis. Ulrich Panne: writing – review & editing, supervision, conceptualization. Carlos Abad: writing – review & editing, validation, supervision, software, resources, project administration, methodology, investigation, funding acquisition, formal analysis, data curation, conceptualization.

Conflicts of interest

There are no conflicts of interest to declare. The system used – a microwave plasma source and a PlasmaQuant MS Elite quadrupole mass spectrometer – was made available by Analytik Jena GmbH.

Data availability

The authors confirm that the data supporting the results of this study are available within the article and its supplementary information (SI). Supplementary information: detailed protocols for setting up chromatographic columns with AG-50W-X8 resin and ion-exchange chromatography for lithium separation; operating parameters for ICP-OES analysis; pre-chromatography lithium concentrations in new and aged cathode/anode materials; lists of lithium samples for quality control with isotope ratios; instrumental parameters for mass spectrometry settings; elution profiles of acid-digested LCO cathodes; and mass scans showing doubly charged ions in blank solutions at varying plasma powers. See DOI: **https://doi.org/10.1039/d4ja00324a**.

Acknowledgements

The authors are thankful to Analytik Jena GmbH for supporting this research. This work was supported by the Bundesanstalt für Materialforschung und -prüfung (BAM) with the funding program "Menschen – Ideen" project numbers IE2120 and MIT1-20-40.

References

1 G. Zubi, R. Dufo-López, M. Carvalho and G. Pasaoglu, The lithium-ion battery: State of the art and future perspectives, *Renewable Sustainable Energy Rev.*, 2018, **89**, 292–308, DOI: **10.1016/j.rser.2018.03.002**.

2 Y. Takami, S. Yanase and T. Oi, Observation of Lithium Isotope Effects Accompanying Electrochemical Release from Lithium Cobalt Oxide, *Z. Naturforsch. A*, 2013, **68**, 73–78, DOI: **10.5560/zna.2012-0080**.

3 Y. Takami, S. Yanase and T. Oi, Lithium Isotope Effects upon Electrochemical Release from Lithium Cobalt Oxide to Non-Lithium Electrolyte Solution, *Z. Naturforsch. A*, 2014, **69**, 97–103, DOI: **10.5560/zna.2013-0080**.

4 K. Okano, Y. Takami, S. Yanase and T. Oi, Lithium Isotope Effects upon Electrochemical Release from Lithium Manganese Oxide, *Energy Procedia*, 2015, **71**, 140–148, DOI: **10.1016/j.egypro.2014.11.864**.

5 R. L. Rudnick, The Little Cation that Could, *Elements*, 2020, **16**, 233–234, DOI: **10.2138/gselements.16.4.233**.

6 P. Tomascak, T. Magna and R. Dohmen, *Advances in Lithium Isotope Geochemistry*, 1st edn, Springer, Cham, 2016.

7 S. Penniston-Dorland, X.-M. Liu and R. L. Rudnick, Lithium Isotope Geochemistry, *Rev. Mineral. Geochem.*, 2017, **82**, 165–217, DOI: **10.2138/rmg.2017.82.6**.

8 Z. C. You, A. Akkus, W. Weisheit, T. Giray, S. Penk, S. Buttler, S. Recknagel and C. Abad, Multielement analysis in soils using nitrogen microwave inductively coupled atmospheric-pressure plasma mass spectrometry, *J. Anal. At. Spectrom.*, 2022, **37**, 2556–2562, DOI: **10.1039/d2ja00244b**.

9 M. Schild, A. Gundlach-Graham, A. Menon, J. Jevtic, V. Pikelja, M. Tanner, B. Hattendorf and D. Gunther, Replacing the Argon ICP: Nitrogen Microwave Inductively Coupled Atmospheric-Pressure Plasma (MICAP) for Mass Spectrometry, *Anal. Chem.*, 2018, **90**, 13443–13450, DOI: **10.1021/acs.analchem.8b03251**.

10 M. Kuonen, G. Niu, B. Hattendorf and D. Gunther, Characterizing a nitrogen microwave inductively coupled atmospheric-pressure plasma ion source for element mass spectrometry, *J. Anal. At. Spectrom.*, 2023, **38**, 758–765, DOI: **10.1039/d2ja00369d**.

11 A. Winckelmann, J. Roik, S. Recknagel, C. Abad and Z. You, Investigation of matrix effects in nitrogen microwave inductively coupled atmospheric-pressure plasma mass spectrometry (MICAP-MS) for trace element analysis in steels, *J. Anal. At. Spectrom.*, 2023, **38**, 1253–1260, DOI: **10.1039/d3ja00088e**.

12 Z. You, A. Akkus, W. Weisheit, T. Giray, S. Penk, S. Buttler, S. Recknagel and C. Abad, Multielement analysis in soils using nitrogen microwave inductively coupled atmospheric-pressure plasma mass spectrometry, *J. Anal. At. Spectrom.*, 2022, **37**, 2556–2562, DOI: **10.1039/d2ja00244b**.

13 J. Jevtic, A. Menon and V. Pikelja, World Intellectual Property Organization, 2014.

14 X.-M. Liu and W. Li, Optimization of lithium isotope analysis in geological materials by quadrupole ICP-MS, *J. Anal. At. Spectrom.*, 2019, **34**, 1708–1717, DOI: **10.1039/c9ja00175a**.

15 S. Juzer, N. Tanwar and S. Misra, Precise determination of lithium isotope ratios at the sub-nanogram level by QQQ-ICP-MS: application to natural waters and carbonates, *J. Anal. At. Spectrom.*, 2022, **37**, 1541–1553, DOI: **10.1039/d2ja00069e**.

16 A. J. Schwartz, Y. Cheung, J. Jevtic, V. Pikelja, A. Menon, S. J. Ray and G. M. Hieftje, New inductively coupled plasma for atomic spectrometry: the microwave-sustained, inductively coupled, atmospheric-pressure plasma (MICAP), *J. Anal. At. Spectrom.*, 2016, **31**, 440–449, DOI: **10.1039/c5ja00418g**.

17 A. Winckelmann, S. Nowak, S. Richter, S. Recknagel, J. Riedel, J. Vogl, U. Panne and C. Abad, High-Resolution Atomic Absorption Spectrometry Combined With Machine Learning Data Processing for Isotope Amount Ratio Analysis of Lithium, *Anal. Chem.*, 2021, **93**, 10022–10030, DOI: **10.1021/acs.analchem.1c00206**.

18 K. Van Hoecke, J. Belza, T. Croymans, S. Misra, P. Claeys and F. Vanhaecke, Single-step chromatographic isolation of lithium from whole-rock carbonate and clay for isotopic analysis with multi-collector ICP-mass spectrometry, *J. Anal. At. Spectrom.*, 2015, **30**, 2533–2540, DOI: **10.1039/c5ja00165j**.

19 A.-M. Desaulty, D. Monfort Climent, G. Lefebvre, A. Cristiano-Tassi, D. Peralta, S. Perret, A. Urban and C. Guerrot, Tracing the origin of lithium in Li-ion batteries using lithium isotopes, *Nat. Commun.*, 2022, **13**, 4172, DOI: **10.1038/s41467-022-31850-y**.

20 S. Juzer, N. Tanwar and S. Misra, Precise determination of lithium isotope ratios at the sub-nanogram level by QQQ-ICP-MS: application to natural waters and carbonates, *J.*

Anal. At. Spectrom., 2022, **37**, 1541–1553, DOI: **10.1039/d2ja00069e**.

21 A. Hineman and C. Stephan, Effect of dwell time on single particle inductively coupled plasma mass spectrometry data acquisition quality, *J. Anal. At. Spectrom.*, 2014, **29**, 1252–1257, DOI: **10.1039/c4ja00097h**.

22 J. Vogl, Calibration strategies and quality assurance, *Inductively Coupled Plasma Mass Spectrometry Handbook*, 2009, pp. 147–181, DOI: **10.1002/9781444305463.ch4**.

23 PerkinElmer, *Advantages of Short Settling Times for Quadrupole-Based ICP-MS Laser Ablation Imaging*, Technical note PerkinElmer, 2020, pp. 1–4,.

24 S. D. Tanner, Space charge in ICP-MS: calculation and implications, *Spectrochim. Acta, Part B*, 1992, **47**, 809–823, DOI: **10.1016/0584-8547(92)80076-S**.

25 R. Thomas, *Practical Guide to ICP-MS*, CRC Press, 2013.

26 R. Thomas, Impact of Measurement Protocol on ICP-MS Data Quality Objectives: Part II, *Spectroscopy*, 2021, **36**, 19–22, DOI: **10.56530/spectroscopy.sd5873x4**.

27 S. S. Dirk Wollenweber and G. Wünsch, Determination of Li, Na, Mg, K, Ca and Fe with ICP-MS using cold plasma conditions, *Fresenius. J. Anal. Chem.*, 1999, **364**, 433–437.

28 M. Kuonen, G. Niu, B. Hattendorf and D. Gunther, Characterizing a Nitrogen Microwave Inductively Coupled Atmospheric-Pressure Plasma Ion Source for Element Mass Spectrometry, *J. Anal. At. Spectrom.*, 2023, **38**, 758–765, DOI: **10.1039/D2JA00369D**.

29 J. Vogl, M. Rosner, S. A. Kasemann, R. Kraft, A. Meixner, J. Noordmann, S. Rabb, O. Rienitz, J. A. Schuessler, M. Tatzel and R. D. Vocke, Intercalibration of Mg Isotope Delta Scales and Realisation of SI Traceability for Mg Isotope Amount Ratios and Isotope Delta Values, *Geostand. Geoanal. Res.*, 2020, **44**, 439–457, DOI: **10.1111/ggr.12327**.

30 DIN, Accuracy (trueness and precision) of measurement methods and results DIN ISO 5725-2, in *Part 2: Basic Method for the Determination of Repeatability and Reproducibility of a Standard Measurement Method*, ISO International Organization for Standardization, 2003.

31 M. Berthault, J. Santos-Peña, D. Lemordant and E. D. Vito, Dynamics of the6Li/7Li Exchange at a Graphite–Solid Electrolyte Interphase: A Time of Flight–Secondary Ion Mass Spectrometry Study, *J. Phys. Chem. C*, 2021, **125**, 6026–6033, DOI: **10.1021/acs.jpcc.0c10398**.

32 Z. Zhang, A. Murali, P. K. Sarswat and M. L. Free, High-efficiency lithium isotope separation by electrochemical deposition and intercalation with electrochemical isotope effect in propylene carbonate and [BMIM][DCA] ionic liquid, *Electrochim. Acta*, 2020, **361**, 137060, DOI: **10.1016/j.electacta.2020.137060**.

33 F. R. Perry, A diffusional contribution to lithium isotope effects, *Biol. Psychiatry*, 1987, **22**, 73–78, DOI: **10.1016/0006-3223(87)90132-6**.

34 D. Santhanagopalan, D. Qian, T. McGilvray, Z. Wang, F. Wang, F. Camino, J. Graetz, N. Dudney and Y. S. Meng, Interface Limited Lithium Transport in Solid-State Batteries, *J. Phys. Chem. Lett.*, 2014, **5**, 298–303, DOI: **10.1021/jz402467x**.

35 S. J. An, J. Li, C. Daniel, D. Mohanty, S. Nagpure and D. L. Wood, The state of understanding of the lithium-ion-battery graphite solid electrolyte interphase (SEI) and its relationship to formation cycling, *Carbon*, 2016, **105**, 52–76, DOI: **10.1016/j.carbon.2016.04.008**.

36 A. Senyshyn, M. J. Muhlbauer, O. Dolotko, M. Hofmann and H. Ehrenberg, Homogeneity of lithium distribution in cylinder-type Li-ion batteries, *Sci. Rep.*, 2015, **5**, 18380, DOI: **10.1038/srep18380**.

37 T. Kim, L. K. Ono and Y. Qi, Understanding the active formation of a cathode–electrolyte interphase (CEI) layer with energy level band bending for lithium-ion batteries, *J. Mater. Chem. A*, 2023, **11**, 221–231, DOI: **10.1039/d2ta07565b**.

